Russian Chemical Reviews **84** (5) 540 – 554 (2015) © 2015 Russian Academy of Sciences and Turpion Ltd

DOI 10.1070/RCR4469

Nanostructured titanium, zirconium and hafnium diborides: the synthesis, properties, size effects and stability

R A Andrievski

Institute of Problems of Chemical Physics, Russian Academy of Sciences
prosp. Akademika Semenova 1, 142432 Chernogolovka, Moscow Region, Russian Federation

The review is concerned with methods of synthesis of nanopowders, nanowires and films based on titanium, zirconium and hafnium diborides. Methods for consolidation of nanoparticles in order to prepare bulk nanostructured samples are analyzed. Information on the physicochemical and physicomechanical properties of these systems is generalized and the role of the size effects is analyzed. Data on the thermal stability and influence of radiation, deformation and corrosion on the TiB_2-, ZrB_2- and HfB_2-based nanostructures are presented. Poorly studied aspects of the title field of research are pointed out.
The bibliography includes 130 references.

Contents

I. Introduction 540
II. Methods of synthesis of nanopowders, consolidated nanomaterials and nanostructured films 542
III. Physicochemical and physicomechanical properties. The size effects and stability 547
IV. Conclusion 552

I. Introduction

Materials based on transition metal borides are chemically inert, refractory and exhibit high hardness and elasticity as well as good electrophysical and nuclear properties. They are used in aerospace industry and nuclear power engineering, friction units and material processing units, chemical engineering, catalysis, electronics and power engineering. The information in this field is rather extensive; representative international symposia on boron, borides and related materials are held every three years. For instance, peer-reviewed papers that were presented at the 17th International Symposium on Boron, Borides and Related Materials held in Istanbul, Turkey, on 11 – 17 September 2011, are available in a special issue of the *Solid State Sciences* journal.[1] However, the properties of boride nanoparticles have been poorly studied so far and relevant information is scarce. A detailed review [2] was solely focused on data on the synthesis of boride nanopowders, while information on consolidated bulk nanomaterials and films, not to speak of their stability, was left out of consideration.[3] Meanwhile, a feature of modern materials science is the increasingly wide use of the nanostructured approach, *viz*., the design of materials whose building blocks are of the order of 100 nm and smaller in size. This makes it possible to significantly improve the physicochemical, physicomechanical and, correspondingly, operating properties of materials and to considerably extend the field of their application.[4]

In this connection it seems appropriate to generalize information on the synthesis and properties of nanostructured materials and to discuss the role of the size effects and the influence of temperature, radiation, deformation and corrosion on their stability taking typical high-temperature diborides TiB_2, ZrB_2 and HfB_2 as examples. It is usually accepted that the maximum grain size in nanomaterials is about 100 nm. For the sake of comparison, we will also provide information for the diboride samples with grains a few micrometres in size.

To make our comparison of the properties of nanostructured and coarse-grained boride materials convenient, it is useful to dwell on recent data on the phase diagrams of B – Ti (Zr, Hf) systems and on the molecular and electronic structures and properties of borides formed in these systems. This is similar to previous analysis of nanomaterials based on SiC and B_4C.[5, 6]

The phase diagrams of metal – boron systems have been studied for more than six decades (see, *e.g*., Refs 7 – 10) and are continuously revised. To date, it is commonly accepted that reactions of Group IV transition metals (M) with boron can result in at least four types of borides including MB, M_3B_4, MB_2 and MB_{12}. Modern phase diagrams of the B – Ti, B – Zr and B – Hf systems (see Fig. 1) are constructed using experimental data and results of thermodynamic

R A Andrievski Doctor of Technical Sciences, Chief Researcher, Group of Nanostructured Materials at the IPCP RAS.
Telephone: +7(496)522 – 7793, e-mail: ara@icp.ac.ru
Current research interests: nanostructured materials science, solid state chemistry and physics, interstitial phases (hydrides, carbides, nitrides, borides).

Received 15 May 2014
Uspekhi Khimii **84** (5) 540 – 554 (2015); translated by A M Raevskiy

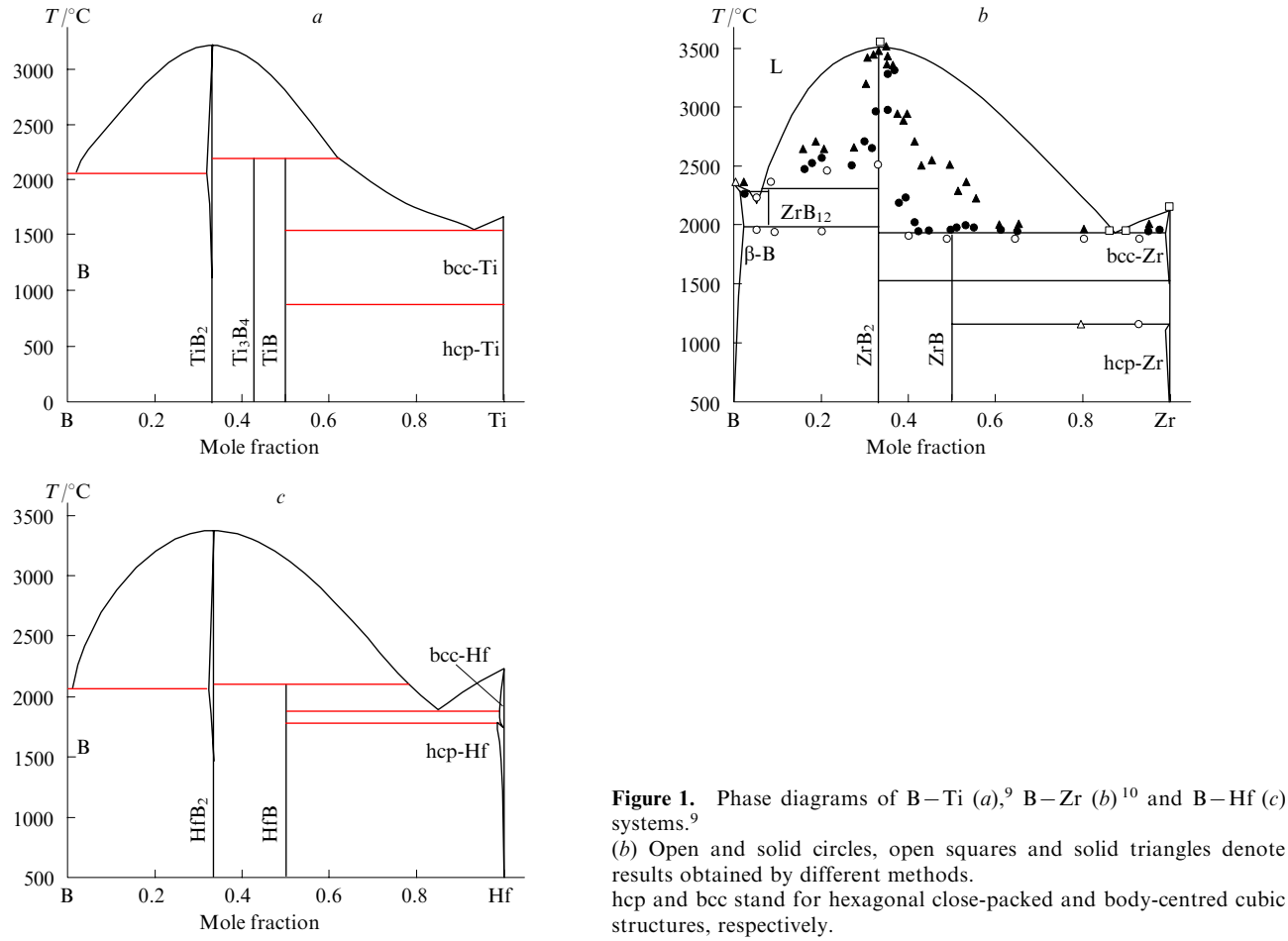


Figure 1. Phase diagrams of B – Ti (*a*),[9] B – Zr (*b*)[10] and B – Hf (*c*) systems.[9]
(*b*) Open and solid circles, open squares and solid triangles denote results obtained by different methods.
hcp and bcc stand for hexagonal close-packed and body-centred cubic structures, respectively.

Table 1. Crystal chemical parameters of titanium, zirconium and hafnium borides.[7,8,11–13]

Boride	Crystal system	Space group	Structural type	Lattice constants /nm			Density /g cm^{-3}
				a	*b*	*c*	
TiB	cubic	*Fm*3*m*	NaCl	0.4245			4.2
TiB	orthorhombic	*Pnma*	FeB	0.612	0.306	0.456	4.58
Ti_3B_4	"	*Immm*	Ta_3B_4	0.304	0.325	1.37	4.56
TiB_2	hexagonal	$P6_3/mmm$	AlB_2	0.3030		0.3230	4.51
ZrB_2	"	$P6_3/mmm$	AlB_2	0.3165		0.353	6.12
ZrB_{12}	cubic	*Fm*3*m*	UB_{12}	0.4408			3.63
HfB_2	hexagonal	$P6_3/mmm$	AlB_2	0.3139		0.3473	11.21
HfB_{12}	cubic	*Fm*3*m*	UB_{12}	0.7371			5.1

calculations. As can be seen, mono- and diborides are present in all systems; the M_3B_4 phases and the decomposing higher boride MB_{12} are not always detected, although structural data for some of them are available (Table 1). Unlike transition metal carbides, nitrides and hydrides,[14] transition metal borides are characterized by very narrow homogeneity regions. For instance, the maximum deviation from stoichiometry for TiB and TiB_2 is ~1 at.%;[15] *i.e.*, the content of structural vacancies influencing the properties of the systems in question is low.

The properties of high-temperature diborides with layered structures comprised of alternating atomic planes of metal and boron (Fig. 2) have been best studied experimen-

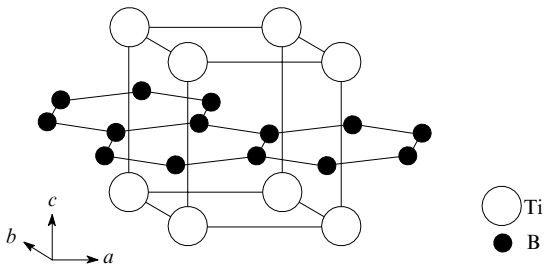


Figure 2. Atomic planes of Ti and B in AlB_2-type hexagonal unit cell.[15]

Table 2. Key physicochemical and physicomechanical properties of titanium, zirconium and hafnium diborides.[12, 15, 16]

Diboride	T_m/°C	E/GPa	H_V/GPa	ρ/μΩ cm
TiB_2	3225	565	24 ± 2	9
ZrB_2	3245	489	23	9.2
HfB_2	3380	480	28	10.6

Note. Notations are as follows: T_m is the melting point, E is the elastic modulus, H_V is the Vickers hardness and ρ is the specific resistance.

tally. The physicomechanical properties of titanium, zirconium and hafnium diborides are presented in Table 2. A detailed analysis of more recent results taking into account the impurity content, grain size, porosity and other factors is available in a handbook.[17] All diborides listed in Table 2 are characterized by high melting points, elastic moduli, Vickers hardness and low specific resistance. It should be noted that the electrical and thermal conductivities of

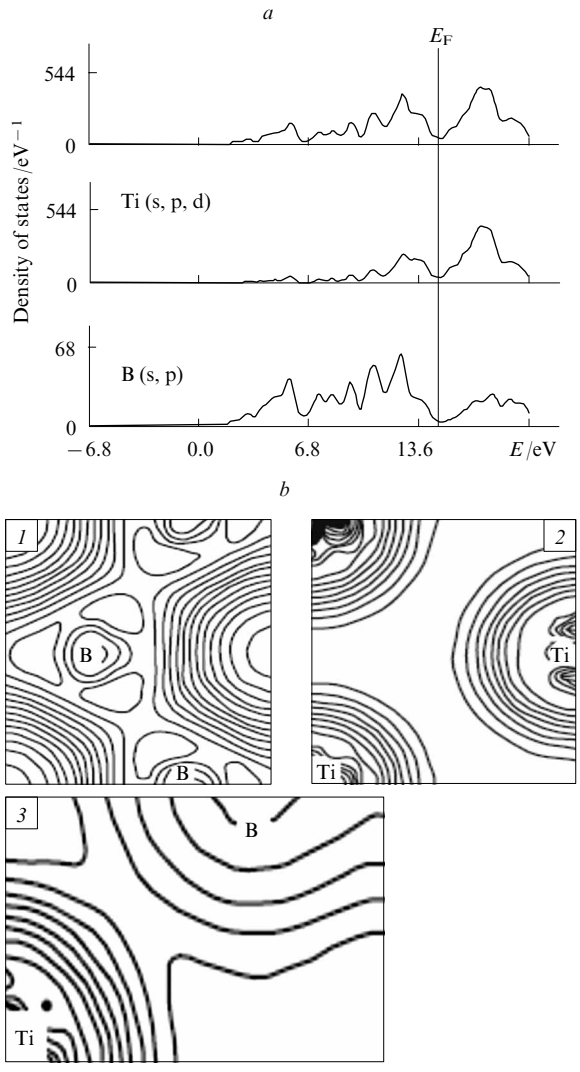


Figure 3. Total density of states and local (Ti and B) densities of states in titanium diboride (*a*) and the charge density distribution (*b*) in the boron (*1*) and titanium (*2*) atomic planes and between these planes (*3*).[18, 19]

diborides are comparable with and even better than those of copper, *i.e.*, diborides are metal-like phases that exhibit the properties of typical brittle compounds (no plasticity), *viz.*, low fracture toughness [K_{IC} = (3–6) MPa m$^{1/2}$], flexural strength (σ_b = 200–400 MPa) and high brittle–ductile transition temperature (⩾2000 °C).[17]

The dual character of the properties of transition metal borides and other refractory transition metal compounds (*e.g.*, carbides and nitrides) is reflected in their electronic energy spectra that were thoroughly studied both theoretically and experimentally (see, *e.g.*, Refs 14 and 17–20). Main features of the electronic spectrum of titanium diboride (Fig. 3 *a*) are as follows:

— the energy bands are degenerate, strongly overlapped and have no band gap;

— the low-energy bonding band mainly originates from strong hybrid interactions of B2p and Ti3d;

— the high-energy antibonding band is only partially filled and originates from Ti–B, B–B and Ti–Ti interactions;

— the Fermi level (E_F) lies between the bonding and antibonding bands and the density of states at E_F is ~59.84 eV^{-1}.

An analysis of the charge density maps (Fig. 3 *b*) revealed the most pronounced overlap for the Ti–B covalent bonds. Also, an electron-donating character of metal atoms was pointed out; *i.e.*, chemical bonds in diborides are characterized by some ionicity. Thus, the metal-like properties of diborides manifest themselves in the electronic energy spectra (no band gap, low density of states at the Fermi level), while the Ti–B covalent bonds are responsible for brittleness and high melting points, elastic properties and hardness.

II. Methods of synthesis of nanopowders, consolidated nanomaterials and nanostructured films

II.1. Selected properties of nanopowders and nanowires

Boride nanopowders can be obtained by vapour-phase reactions, carbothermal synthesis, decomposition of compounds (*e.g.*, borohydrides), high-energy ball milling and mechanochemical synthesis.[21, 22] Studies on the synthesis of boride nanopowders have been significantly extended (see, *e.g.*, a review [2]). Recent data concerning the preparation of titanium, zirconium and hafnium diboride nanopowders and nanowires are collected in Table 3 where the references are arranged chronologically to demonstrate increasing interest in the synthesis of the nanostructures in question.

Many researchers are interested in the ZrB_2- and HfB_2-based nanomaterials as basic components of ultrahigh-temperature composites capable of operating under extreme conditions (at very high temperatures, under high mechanical stress and in corrosive media).[12, 52] Studies on the reinforcing additives are extended. In particular, lightweight matrix composites Al–TiB_2, which are promising for aerospace and automotive industries, *etc.*,[53] are obtained using titanium diboride nanoparticles prepared by high-energy ball milling of commercially available TiB_2 powders or by mechanochemical synthesis from mixtures of elemental Ti and B powders (Ti + 2 B).

Table 3 lists the key characteristics of different methods of synthesis and corresponding starting components. A number of general, thermodynamically feasible high-tem-

Table 3. Methods of synthesis of boride nanopowders and nanowires.

Boride	Nanoparticle size and CSR size [a] /nm	Method of synthesis	Starting components	T/°C	Ref.
ZrB_2	20 – 50 (diameter), ~600 (length)	carbothermal reduction in molten salt	$ZrO_2 + H_3BO_3 + C + NaCl +$ + catalyst (Fe/Ni/Co)	1500 – 1700	23
TiB_2	15 – 60 3 – 5 (see [b])	mechanochemical synthesis (high-energy ball milling)	$TiCl_3 + LiBH_4 + LiH$	–	24
TiB_2	~270	the same	$TiO_2 + B_2O_3 + Mg$	–	25
TiB_2	100 – 400	metallothermic reduction using Mg	$TiO_2 + B_2O_3 + Mg$	800	26
ZrB_2	70 – 200	self-propagating high-temperature synthesis using molten salts	Zr + B + NaCl	300 – 1000 (see [c])	27
ZrB_2	< 100	mechanochemical synthesis (attritor ball milling followed by hot pressing)	Zr + B	600	28
TiB_2	10 – 20 (diameter), 50 – 80 (length)	high-energy ball milling TiB_2 (fabrication of bicephalous nanowires)		–	29
ZrB_2	150 – 660	borothermal reduction	$ZrO_2 + B + H_3BO_3$	1000 – 1650	30
HfB_2	~2.5	electron-beam deposition *via* decomposition of $Hf(BH_4)_4$ on Si(100) (fabrication of nanowires)		20	31
HfB	50	synthesis in molten salts	$HfCl_4 + NaBH_4 + LiCl + KCl$	800	32
TiB_2	20 – 100	plasma-chemical synthesis	$TiO_2 + B_2O_3 + CH_4$	–	33
TiB_2	20 – 45 (see [b])	the same	Ti + B	$(2 – 3) \times 10^3$	34
TiB_2	25 – 50	electrochemical synthesis in molten salts	$Ti + B_2O_3 + CsCl + NaCl$	540 – 570	35
$(Ti,Zr)B_2$ $(Ti,Hf)B_2$	20 – 60 (see [b]) 20 – 40 (see [b])	mechanochemical synthesis (high-energy ball milling)	Ti + Zr + B; Ti + Hf + B	–	36
HfB_2	800	borothermal reduction	$HfO_2 + B$	1100	37
HfB_2	100 – 200	carbothermal reduction	$HfO_2 + B_2O_3 + C$	1500	38
ZrB_2	~10 (see [b])	high-energy ball milling of ZrB_2			39
ZrB_2	100 – 2100 (diameter), 40 – 200 (length)	mechanochemical synthesis followed by heating	$ZrCl_4 + B$	1200	40
TiB_2	35 – 50	synthesis in molten salts	$Ti + B + Na_2B_4O_7$	815	41, 42
ZrB_2	90 – 95	the same	$Zr + B + Na_2B_4O_7$	750 – 850	43
ZrB_2	50 – 500	high-energy ball milling of ZrB_2		–	44
ZrB_2	200 – 300	mechanochemical synthesis	Zr + B		45
ZrB_2	200	carbothermal reduction (synthesis of nanofibres *via* electrospinning)	polyzirconoxane + H_3BO_3 + + polyacrylonitrile	1500	46
TiB_2	$1 – 5 \cdot 10^3$	carbothermal reduction (synthesis of micropowders with plate-like particles)	$TiO_2 + H_3BO_3 + C$	1000 – 1400	47
TiB_2	~140	mechanochemical self-propagating synthesis (high-energy ball milling)	$TiO_2 + B_2O_3 + Mg + NaCl$	–	48
TiB_2	3 – 83	plasma-chemical synthesis	TiB_2; Ti + B; Ti + B + C	$(3 – 4) \times 10^3$	49
ZrB_2	> 200	carbothermal reduction	$ZrOCl_2 \cdot 8H_2O + B(C_2H_5O)_3 +$ + $[(HOC_6H_4)_2CH_2]_n$	1500	50
HfB_2	> 200	the same	$HfOCl_2 \cdot 8H_2O + B(C_2H_5O)_3 +$ + $[(HOC_6H_4)_2CH_2]_n$		
HfB_2	30 – 150	"	$51\,HfCl_4 + H_3BO_3 +$ + $[(HOC_6H_4)_2CH_2]_n$	1300 – 1600	51

[a] Coherent scattering region (CSR). [b] Data for CSR. [c] Listed are the values calculated from the adiabatic temperatures of self-propagating high-temperature synthesis.

perature reactions of synthesis of diborides can be written as follows: [23 – 25, 31, 37, 40]

$$ZrO_2 + B_2O_3 + 5\,C \longrightarrow ZrB_2 + 5\,CO\uparrow \quad (1)$$

$$TiCl_2 + 2\,LiBH_4 + LiH \longrightarrow TiB_2 + 3\,LiCl + 4.5\,H_2\uparrow \quad (2)$$

$$TiO_2 + B_2O_3 + 5\,Mg \longrightarrow TiB_2 + 5\,MgO \quad (3)$$

$$Hf(BH_4)_4 \longrightarrow HfB_2 + B_2H_6\uparrow + 5\,H_2\uparrow \quad (4)$$

$$3\,HfO_2 + 10\,B \longrightarrow 3\,HfB_2 + 2\,B_2O_3\uparrow \quad (5)$$

$$3\,ZrCl_4 + 10\,B \longrightarrow 3\,ZrB_2 + 4\,BCl_3\uparrow \quad (6)$$

These reactions are written in their final form, although in fact, they are essentially multistage. For instance, boric acid (typical starting compound) heated to 200–300 °C undergoes dehydration and is transformed to B_2O_3 which in turn undergoes melting at ~450 °C and evaporates with ease. Boric acid can also react with solid boron to give gaseous B_2O_2, *etc.*[37,47]

When performing the synthesis one goal is to reduce the reaction temperature (*e.g.*, melt synthesis,[32,35,41–43] high-energy ball milling and mechanochemical synthesis,[24,25,28,29,36,39,44,45,48] self-propagating high-temperature synthesis with inert filler[27] or combinations of different methods[25,48]) and thus obtain products with small particle size. On the other hand, researchers aim to improve the performance of synthetic procedures (plasma synthesis methods have the highest performance).[33,34,49] Attempts to replace high-energy ball milling by the sol–gel method were reported.[50,51] Considerable attention is paid to cleaning the end products from related substances (*e.g.*, salts in the case of melt synthesis;[32,35,41–43] magnesium oxide in the case of metallothermic reduction using Mg[25,26,48]); however, abrasion damage accompanying high-energy ball milling is almost unavoidable. Nanopowders exhibit high surface activity; therefore, one should use protective inert media to prevent oxidation of the samples.

Certification of the size and chemical composition of nanoparticles is performed by X-ray phase analysis (XRD), scanning electron microscopy (SEM) and transmission electron microscopy (TEM) including high-resolution TEM, by X-ray photoelectron spectroscopy (XPS), energy dispersive X-ray spectroscopy (EDS), secondary-ion mass spectroscopy (SIMS), Rutherford back-scattering spectroscopy and Auger electron spectroscopy (AES). Qualitative phase analysis and detection of temperature-induced transformations are carried out by Raman spectroscopy, IR spectroscopy, differential thermal analysis and by plotting thermogravimetric analysis (TGA) curves. The specific surface area of nanopowders is measured by the Brunauer–Emmett–Teller (BET) method. The size of the coherent scattering regions (CSR) is evaluated by XRD and independently by the TEM (SEM) and BET methods; a comparison of the results thus obtained helps to make the certification of nanoparticles more reliable.

The SEM and TEM images of (i) TiB_2 and HfB_2 nanoparticles prepared by high-energy ball milling[24] and carbothermal reduction[38] and (ii) ZrB_2 nanowires synthesized by carbothermal reduction *via* electrospinning are shown in Fig. 4 *a*–*c*. The EDS data (see Fig. 4 *d*) point to the presence of oxygen impurity and to nonstoichiometric composition of the nanowires. Assuming that oxygen atoms are in some way arranged in the boron sublattice (see Fig. 2), the approximate chemical composition is $Zr(B_{0.95}O_{0.05})_{1.97}$. A morphological analysis revealed both round and faceted diboride particles; besides, agglomeration of nanopowders and nanowires is often observed (see Fig. 4 *b* and *c*).

The lattice constants of particles of TiB_2 and ZrB_2 nanopowders synthesized by different methods[24,40,41,43] slightly deviate from the tabulated (recommended) values (see Table 1). This can be due to the presence of impurities and defects originating from deformation (*e.g.*, ball milling). The XPS spectra exhibit not only lines typical of TiB_2 and ZrB_2, but also weak lines corresponding to the metal and boron oxides and to elemental boron.[42,43]

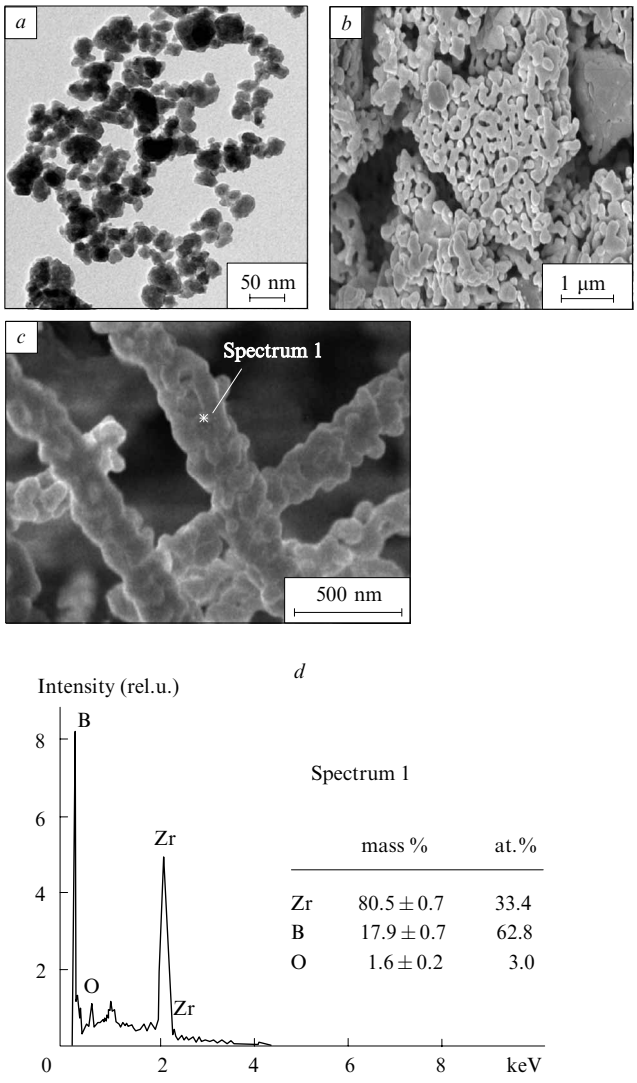


Figure 4. Electron micrographs: TiB_2 nanopowder (*a*),[24] HfB_2 nanopowder (*b*),[38] ZrB_2 nanowires (*c*); EDS spectrum and elemental composition of ZrB_2 (*d*).[46]

The influence of various factors on the synthesis of TiB_2 was thoroughly studied by diverse methods and approaches.[34,42,45,47–49]

A detailed investigation of the synthesis of TiB_2 micropowders by carbothermal reduction of titanium and boron oxides at 1000–1400 °C made it possible to monitor how the heating rate and the duration of keeping under isothermal conditions influence the degree of reaction completion and the phase and morphological compositions of reaction products.[47] Titanium diboride powders prepared at 1300 °C contained about 6% of oxycarbide TiC_xO_y. A scanning electron microscopy (SEM) study revealed the growth terraces on the surface of hexagonal diboride particles; this is indicative of the autoepitaxial growth mechanism with transfer of components through the gas phase.[47]

According to XRD data, the feed rate of Ti and B powders to high-frequency plasma and the Ti/B ratio influence the size of TiB_2 particles and the proportion of the monoboride TiB in the mixture with TiB_2 (Fig. 5); here, the proportion of the unreacted amorphous boron was

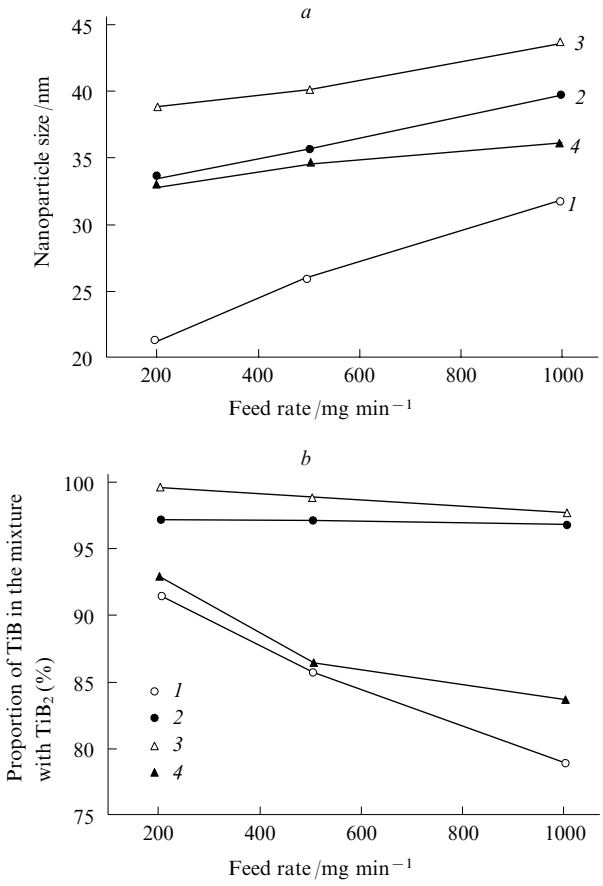


Figure 5. Effect of Ti and B powder feed rates and Ti : B ratio on the size of prepared TiB_2 nanoparticles (*a*) and on the proportion of TiB in the mixture with TiB_2 (*b*).[34]
Ti : B ratio: 1 : 1 (*1*), 2 : 1 (*2*), 3 : 1 (*3*) and 3 : 2 (*4*).

ignored.[34] Carrying out plasma-chemical synthesis of TiB_2 nanopowders with specified particle size requires that many engineering factors be taken into account. A study[49] on the plasma-chemical synthesis of TiB_2 using a wide range of solid precursors (TiB_2, $Ti + 2B$, $TiO_2 + 4B$ and $TiO_2 + 3B + 3C$) showed that the compositionally best TiB_2 nanopowders (purity 97%) with nearly 45-nm particles can be prepared from commercially available TiB_2 powder with particles 1 – 7 μm in size. Thermodynamic calculations for the temperature interval from 500 to 7500 K predict that feasible melting of diboride particles followed by evaporation is expected in the temperature range from 2900 to 3800 K while condensation and crystallization of solid particles are expected in the range from 500 to 2900 K.

By and large, the mechanisms of formation of diboride micro- and nanopowders using different methods of synthesis have been studied insufficiently (particularly, the melt synthesis[32, 35, 41 – 43]); further investigations are required. A comparison of different methods of synthesis (see Table 3) as well as thorough discussion of the physicochemical and service properties of nanopowders synthesized and a detailed comparison of technical and economic parameters are still a matter of the future. As far as we know, only two companies, US Research Nanomaterials, Inc. (www.us-nano.com) and NaBond Technologies Co. (www.nabond.com, with the head office in Hong Kong), produce TiB_2 and ZrB_2 nanopowders (particle size 40 – 60 nm, purity > 95% – 99%) using the plasma technology. The former company delivers its production in lots (1-, 5-, 25-, 100-g lots and more).

II.2. Preparation of consolidated nano- and micromaterials

Covalent character of chemical bonds in diborides and, correspondingly, low diffusional and dislocation mobilities in them predetermine the need for high-temperature sintering to obtain dense samples. The temperature at which active sintering of TiB_2, ZrB_2 and HfB_2 powders begins should be higher than $\sim 0.55\,T_m$, or > 1800 °C.[54] Hot pressing activates densification of powders. Numerous experimental data (see, *e.g.*, Refs 51 and 52) mainly confirm these estimates. Taking hot-pressed (2000 – 2100 °C) commercially available ZrB_2 powders (H C Starck, Germany) with particles 1.5 – 3 μm in size as examples,[55] it was shown that small additives of carbon and zirconium hydride favour removal of oxygen and B_2O_3 and lead to more intense densification and, correspondingly, to higher relative density of samples, which can be as high as 96% – 99%. However, the grain size is 7 – 10 (2000 °C) and 12 – 16 μm (2100 °C).

Using nanopowders, one can reduce the active sintering temperature,[53] but grain growth and degradation of the nanostructure under the sintering conditions and even hot pressing remains unavoidable. The relative density and grain size of TiB_2 nanopowders (US-Nano, USA) are plotted *vs.* microwave sintering temperature in Fig. 6. As can be seen, intense grain growth accompanied by disappearance of the nanostructure begins at 1600 °C even at a

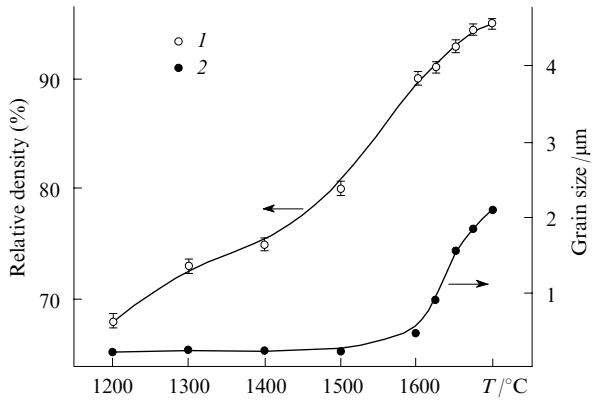


Figure 6. Effect of sintering temperature (dwell time 10 min) on the relative density (*1*) and grain size (*2*) of TiB_2 samples (particle size in the starting nanopowders was ~30 nm and the oxygen concentration was < 1.9%).[56]

porosity of 20%.

At present, spark plasma sintering (SPS)† of nanopowders is gaining ground. In this method, a sample being sintered is compressed at 50 – 100 MPa and pulsed d.c. (1 – 5 kA, pulse duration ~3 ms) is passed simultaneously;

† The method is also known as plasma activated sintering (PAS).

the sintering temperature can be as high as 2400 °C at a heating rate of 500 °C min^{-1}. Owing to the development of high local temperatures in the inter-grain space the method enables more intense densification and low porosity at a relatively small duration of the process, which favours a less intense grain growth and partial retention of nanostructure.

The results of SPS studies of ZrB_2 and HfB_2 nanopowders showed [44, 51, 57] that one can prepare samples with a porosity of 2% to 6% and a grain size ranging from 0.2 to 2 μm. A comparison of SPS and hot pressing of TiB_2 powders with ~1.1-μm particles led to a complicated situation.[58] In the former case, samples with a porosity of 2.5% were prepared at a sintering temperature that was 400 °C lower than in the latter case (grain size was 2–3 μm for SPS and 3–5 μm for hot pressing). Besides, XRD revealed the formation of an additional phase (orthorhombic monoboride TiB, see Table 1) only in the samples prepared by SPS; this also manifested itself in different physicomechanical properties of the samples. Presumably, the formation of TiB is due to insufficient requirements for vacuum hygiene under SPS conditions and to the possibility for the oxidation of TiB_2 to occur in the reaction

$$4\,TiB_2 + 3\,O_2 \longrightarrow 4\,TiB + 2\,B_2O_3 \quad (7)$$

According to thermodynamic calculations, TiB can also form in the reaction

$$TiB_2 + TiO_2 + 2\,C \longrightarrow 2\,TiB + 2\,CO \quad (8)$$

which can proceed at $T > 1600$ °C provided that the starting powders contain TiO_2 and free carbon as impurities.

It was proposed to use SPS when densification is combined with reactive synthesis to prepare ZrB_2-SiC microstructured composites from a preliminarily high-energy ball milled mixture of powders $2\,Zr + Si + B_4C$.[59] Studies on the influence of various additives (Ti, $MoSi_2$, SiC and other compounds for activation of sintering) on the intensification of SPS of refractory diborides were reported.[51, 52, 60]

As applied to hot pressing and SPS of ZrB_2 powders, attempts were undertaken to replace initial random distribution of particles by certain ordered patterns using colloidal processing,[61] texturing by slip casting [62] and magnetic texturing.[63] After slip casting, extended zirconium diboride particles (2–5 μm in diameter and 10–25 μm long) are hot pressed at 2000 °C at a pressure of 30 MPa.[62] A magnetic field of 12 T was also used for texturing ZrB_2 and ZrB_2 + $MoSi_2$ samples.[63]

At present, methods for consolidation of boride nanopowders (see above) do not provide a complete retention of nanostructure; additional search for optimum conditions are required.

II.3. Synthesis of nanostructured films

Compared to the preparation of consolidated boride powder nanomaterials, advances in the synthesis of nanostructured films and coatings based on borides are more pronounced (see, *e.g*, a reviews [21, 22, 64–66] and a book [67]). Systems based on titanium diboride have been best studied. TiB_2, ZrB_2 and HfB_2 films up to a few micrometres thick can be obtained by chemical vapour deposition (CVD) and physical vapour deposition (PVD) and by combined methods. In the former case, the following reactions are used:[52, 64]

$$MCl_4 + 2\,BCl_3 + 5\,H_2 \longrightarrow MB_2 + 10\,HCl \quad (9)$$

$$M(BH_4)_4 \longrightarrow MB_2 + B_2H_6 + 5\,H_2 \quad (10)$$

Environmentally hazardous features of reaction (9) as well as high reactivity and toxicity of borohydrides make CVD of limited use compared to PVD which has recently been a subject of increasing interest.[64–67]

Nevertheless, studies of HfB_2 films deposited upon decomposition of $Hf(BH_4)_4$ on different substrates in a wide temperature range led to some new results.[68–70] In particular, the ⟨0001⟩ dominant texture is characteristic of the deposition on amorphous substrates (SiO_2) at temepatures below 700 °C; at higher temperatures, the $\langle 10\bar{1}0\rangle$ orientation is observed.[68] A similar situation occurs in the case of deposition on the (001) plane of single-crystalline silicon, but the ⟨0001⟩ texture was detected at all temperatures of film deposition on the Si(111) substrates. The growing HfB_2 crystals had a columnar structure at low temperatures of deposition on SiO_2 and a random structure at deposition temperatures $\geqslant$ 800 °C. The crystals were ~10–20 nm across and the film thickness was 300–400 nm.

A XRD study on film growth in argon atmosphere containing a small amount of nitrogen (total pressure was 0.49–0.85 Pa) revealed a mixture of phases HfB_2 + HfN + BN in the amorphous films deposited at $T < 350$ °C and annealed at $T > 600$ °C.[69] Also, the use of a growth inhibitor (NH_3) allows one to homogenize nucleation and subsequent growth and thus obtain smooth thin films.[70] The morphological features of the surface seen in the SEM image and the peak height distribution for HfB_2 films are presented in Fig. 7. In the presence of ammonia, the maximum peak height decreases by a factor of nearly 2.5. Smooth films are promising as diffusion barriers for microelectronics.[70]

A detailed study of the structure and properties of HfB_2 and HfB_2 + BN films prepared by high-frequency nonreactive (Ar) and reactive (Ar + N_2) magnetron sputtering was reported.[71] Films 1–2 μm thick were deposited onto hard-alloy (T15K6) and steel (12X18H9) substrates heated to 550 °C. Four types of film structures were obtained by varying the substrate temperature and bias potential (by varying the energy of Ti and B ions being deposited):

— highly textured columnar structure ⟨0001⟩ with CSR 20–30 nm in size;

— weakly textured columnar structure ⟨0001⟩ with CSR 15–20 nm in size;

— random nanocrystalline structure ('cluster structure' in the original study [71]) with CSR 10 nm in size; and

— amorphous structure.

Figure 8 presents the profiles of the (B/Hf) ratio in the film structures mentioned above (SIMS data). Changes in the lattice constants can be illustrated as follows:

— $a = 0.3179$, $b = 0.365$ nm for the highly textured film;

— $a = 0.323$, $b = 0.340$ nm for the film with random nanocrystalline structure.

These values (see also Table 1) show that the influence of the structure on the film properties should be analyzed taking into account the role of the chemical composition.

Although titanium diboride films have been thoroughly studied earlier,[65] intensive research into these systems con-

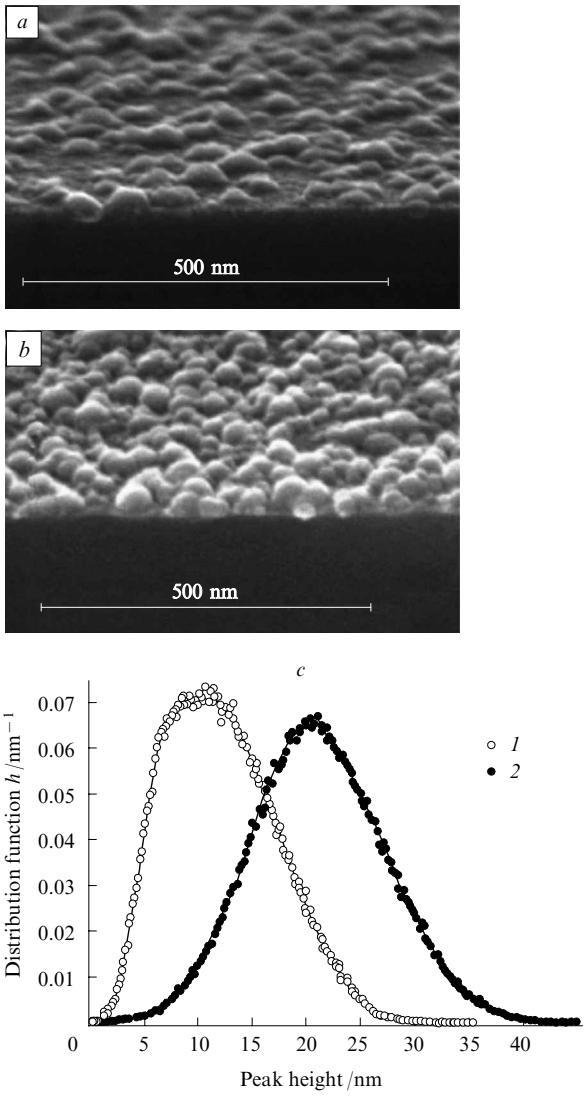


Figure 7. SEM images of the surface of HfB_2 films grown with inhibitor (*a*) and without inhibitor (*b*); peak height (*h*) distributions (atomic force microscopy data) for these conditions (*c*): curve *1* for (*a*) and curve *2* for (*b*).[70]

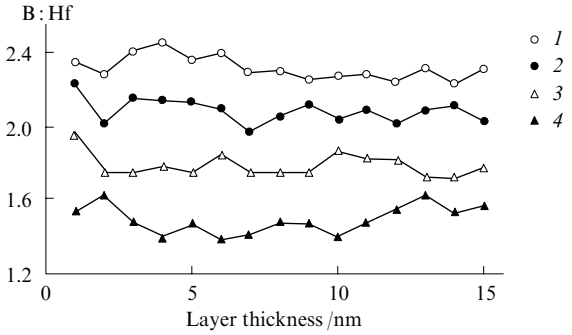


Figure 8. Concentration profiles of B : Hf ratio for HfB_2 films with highly textured (*1*), weakly textured (*2*), random nanocrystalline (*3*) and amorphous (*4*) structures (total film thickness is about 100 nm).[71]

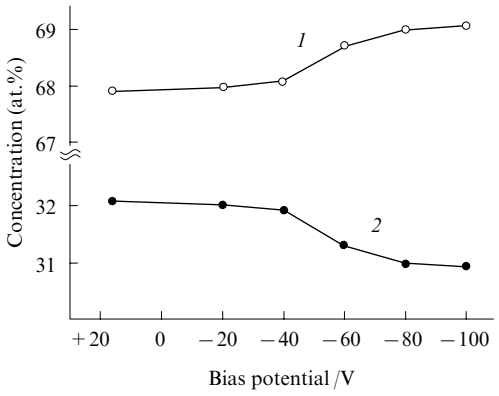


Figure 9. Effect of the bias potential on the concentrations of boron (*1*) and titanium (*2*) in TiB_2 films.[73]

tinues. New results were obtained and other factors influencing the structure formation, chemical composition, stressed state and properties of magnetron sputtered TiB_2 films were analyzed.[72–77] These factors include the energy of ions being condensed (control by varying the bias potential and ion current), the substrate temperature and the substrate rotation rate, pulsed regimes and the type of electric current, the presence of buffer, gradient and intermediate layers, the influence of external magnetic field, specific features of ion implantation and reflection, *etc.*[72,73,75,76] The concentrations of titanium and boron in films (AES data) are plotted *vs.* bias potential in Fig. 9.[73] It is believed that TiB_2 films prepared by d.c. magnetron sputtering on a substrate heated to 550 °C at a negative bias potential of − 50 V exhibit the highest hardness and adhesive strength.[72] Films thus prepared are characterized by a highly textured structure ⟨0001⟩, a crystallite size of 20 nm and minimum residual compressive stress.

A similar series of studies on the influence of diverse factors on the structure formation, chemical composition and properties of magnetron sputtered zirconium diboride films was reported.[72] Specific features of the deposition of ZrB_2 films upon decomposition of $Zr(BH_4)_4$ and magnetron sputtering include a less pronounced effect of the substrate temperature and bias potential on the deviation from stoichiometry, texture and electrical properties of the films.[78–80]

Among the mixed CVD/PVD methods, mention may be made of a study on the properties of superhard TiN/BN/TiB_2 nanocomposite films prepared in high-frequency plasma from a $TiCl_4 + BCl_3 + N_2 + H_2$ mixture.[81] These films are characterized by high hardness, thermal stability and oxidation resistance; they contain amorphous boron nitride and titanium diboride phases and TiN nanocrystals.

III. Physicochemical and physicomechanical properties. The size effects and stability

III.1. Sublattice population. The phase diagrams

As mentioned above, the deviation from stoichiometry for titanium, zirconium and hafnium diborides under equilibrium conditions is very small (see Fig. 1). Atoms deposited under nonequilibrium conditions by CVD and especially PVD can have rather high energies; therefore, the state of

Table 4. Selected parameters of nonstoichiometric titanium and hafnium diboride films prepared by d.c. (DC) and high-frequency (HF) magnetron sputtering.

Approximate formula	Structural type	Lattice constants /nm		Grain size /nm	Regime	Bias potential /V	Ref.
		a	*c*				
Method of determination: AES							
$Ti(B_{0.73}N_{0.2}O_{0.05}C_{0.02})_{1.56}$	AlB_2	0.3060	0.3201	4–8	DC	30	21
$Ti(B_{0.69}N_{0.24}O_{0.04}C_{0.03})_{1.64}$	AlB_2	0.3083	0.3246	3.6 ± 1.8	HF	0	21
$Ti(B_{0.56}N_{0.29}O_{0.05}C_{0.1})_{1.32}$	AlB_2	0.3005	0.3263	2.3 ± 1.1	HF	0	21
$Ti(B_{0.34}N_{0.49}O_{0.12}C_{0.05})_{1.49}$	NaCl	~0.42		2.9 ± 1.5	HF	0	21
$TiB_{2.23}$	AlB_2	0.3045	0.3260	7–15	HF	−100	73
Method of determination: SIMS							
$HfB_{2.3-2.4}$	AlB_2	0.3179	0.3560	20–30	DC	50	71
$HfB_{1.4-1.5}$	amorphous				DC	−50	71

the nanocrystalline structures being formed will be far from equilibrium. Studies on the composition of diboride films point to the possibility of formation of under- and superstoichiometric phases in the nanosized systems (Table 4). Additional information on TiB_2 and ZrB_2 films can be found in reviews.[65, 72] The data in Table 4 show that by varying the bias potential (*i.e.*, by controlling the ion deposition rate) one can prepare diboride films with a considerable deviation from stoichiometry. In this connection a question arises as to how the boron and metal sublattices are filled. In the case of understoichiometric phases it is natural to assume the formation of structural vacancies in the boron sublattice. For superstoichiometric phases, the following situations are possible:

— formation of structural vacancies in the metal sublattice,

— incorporation of extra boron atoms into the boron sublattice, and

— the presence of excess boron atoms at numerous interfaces in the nanostructure.

The authors of HR TEM studies[82, 83] of superstoichiometric titanium diboride ($TiB_{2.4}$) films proposed the following columnar structure of this system (Fig. 10): about 20-nm wide diboride columns have a ⟨0001⟩ dominant texture and boron-rich boundaries; the columns are composed of smaller stoichiometric TiB_2 subcolumns with an average diameter of about 5 nm; the subcolumns are separated by boron-rich 'tissue phase' ~0.5 nm thick. The content of boron at the interfaces was determined by electron energy loss spectroscopy.

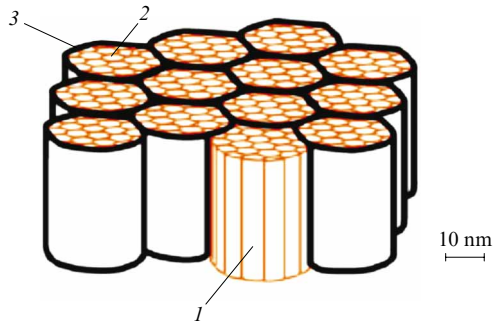


Figure 10. Schematic representation of the columnar structure of superstoichiometric titanium diboride ($TiB_{2.4}$) films.[82, 83]
Stoichiometric TiB_2 nanocrystals ('subcolumns') (*1*); boron-rich boundaries of large columns (*2*) and boron-rich interfaces between TiB_2 nanocrystals ('tissue phase') (*3*).

According to density functional theory calculations of the structure of TiB_2,[73] boron atoms can appear in bulk interstices (see Fig. 2) and form cluster inclusions or boron segregation at interfaces can occur.

In addition to neutron structural analysis (which could be implemented by synthesizing nanoparticles using the ^{11}B isotope characterized by a small thermal neutron capture cross-section) a possible independent method for determining the sublattice filling in superstoichiometric films is to measure the X-ray and picnometric density; however, corresponding thin film studies are hardly feasible.

As far as we know, the phase diagrams of B–M nanosystems have been studied neither theoretically nor experimentally. For quasi-binary systems TiB_2–TiN (or TiC) and TiB_2–B_4C, rough calculation in the regular solution approximation revealed the influence of the nanostructure on the decrease in the eutectic temperature (ΔT_E).[4, 66] Using the expressions for partial Gibbs free energies of the system in the liquid and solid state (in the latter case, taking into account the excess grain-boundary surface energy), the following relationships characterizing the influence of the dispersion of components on ΔT_E were derived:

$$\Delta T_E = \frac{\Delta G_2}{R \ln x} \tag{11}$$

$$\Delta T_E = \frac{\Delta G_2}{(R \ln x_E - \Delta S_{m2})} \tag{12}$$

$$\Delta T_E = \frac{\Delta G_2}{(1 - x_E)/(1 - x) - \Delta S_{m1})} \tag{13}$$

where ΔG_i is the contribution of the excess grain-boundary surface energy calculated per mole

$$\Delta G_i = \frac{6 V_i \sigma_i}{L_i}$$

V_i is the molar volume, σ_i is the grain-boundary surface energy, x and x_E are the concentrations at the limiting

Table 5. Reduction of eutectic temperature (ΔT_E, K) in TiB_2-TiN(-TiC) and TiN(TiC) – TiB_2 pseudobinary systems at different degree of dispersion of the second component.[84]

L /nm	$TiB_2-TiN(TiC)$	$TiN(TiC)-TiB_2$
200	35	45
100	70	90
20	350	450
10	700	900

Note. Coarse-grained samples of the TiB_2-TiC and TiB_2-TiN systems are characterized by T_E = 2790 and 2870 K, respectively.[17]

Table 6. Reduction of eutectic temperature for films in the TiB_2-B_4C system at different grain size (L) and different grain-boundary surface energy (σ).[85]

σ /J m^{-2}	L = 5 nm	L = 10 nm
3	1000	500
2	670	340
1	340	170

Note. Coarse-grained samples have T_E = 2580 K.

solubility and eutectic, respectively; ΔS_{mi} is the entropy of melting and L_i is the inclusion (grain) size.

Relationships (11) – (13) are equivalent and their practical use depends on the availability of particular data for the components 1 and 2. The ΔT_E and T_E values calculated for the TiB_2-TiN, TiB_2-TiC and TiB_2-B_4C systems are listed in Tables 5 and 6. It follows that noticeable decrease in the eutectic temperature is observed if the particle size of the dispersed component is of the order of a few tens of nanometres. The grain-boundary surface energies of these systems are unknown; therefore, Table 6 lists the results calculated for three probable σ_i values (the data in Table 5 were calculated for σ_i = 3 J m^{-2}). Figure 11 presents a tentative phase diagram for TiB_2-TiN film samples with nearly 10-nm grains (dashed lines) constructed taking into account the phase composition of the films studied (see Refs 86 and 87); for comparison, the equilibrium phase diagram [17] is also plotted.

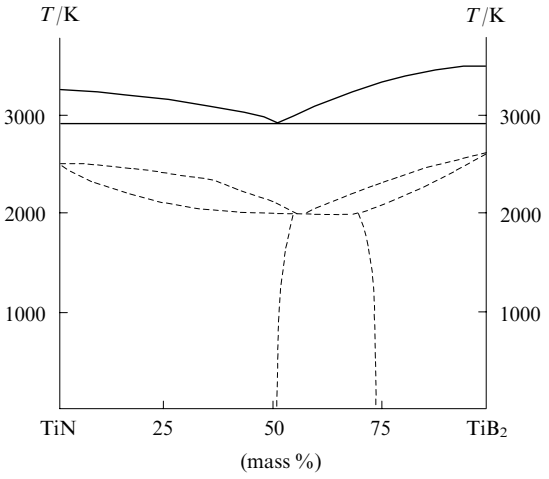


Figure 11. Phase diagram of the $TiN-TiB_2$ system for coarse-grained samples (solid lines) and films (grain size ~10 nm; dashed lines).[84]

Of course, one should keep in mind that we deal with rough estimates because of limitations within the framework of the regular solution approximation and uncertainty in σ values. Nevertheless, the results obtained can be useful for estimating the upper bound of the operating temperatures in the design of high-temperature materials (for, *e.g.*, high-temperature structures, high-temperature friction units and materials processing units) based on nanocrystalline refractory compounds.

III.2. Physicomechanical properties

Key physicomechanical properties of the diborides under study and composites based on them are listed in Table 7. In the case of nanosized samples, the hardness, elastic and electrical properties were determined for film samples only. Corresponding data for sintered samples were mainly obtained for diboride compositions (grain size of the order of a few micrometres) containing additives for intensification of sintering.

When analyzing the data in Table 7, one should keep in mind that they were obtained by different methods and are hardly comparable in some cases. For instance, film hardness values should be compared taking account of possible influence of substrates, the type of indenter and character of load, as well as the surface roughness, possible residual stress, *ets*. Besides, the Vickers hardness values determined in the nanoindentation experiments are usually lower than corresponding values calculated from the indentation area owing to relaxation phenomena upon unloading (see, *e.g.*, Ref. 89). Taking into account the aforesaid, one can suggest that the role of the grain size can be analyzed only qualitatively. Nevertheless, a comparison of the data for at least titanium diboride (best studied phase) and, to some extent, for hafnium diboride (see Tables 2 and 7) shows that going to the nanostructure is accompanied by an increase in hardness and a decrease in the Young modulus; this correlates with the known laws of changes in H_V and E for various types of nanomateirials.[4, 100] On the one hand, an increase in the proportion of grain boundaries (interfaces) acting as stoppers for cracks and dislocations increases the strength and hardness. On the other hand, the amount of intercrystallite (amorphous) phase with poor elastic properties increases and the elastic modulus correspondingly decreases. In particular, an increase in H_V and a decrease in E are well illustrated by the data for films Nos 1 – 5, 11, 28 and 29 (see Table 7).

The electrical resistance of nanofilms is much higher than that of coarse-grained films owing to charge carrier scattering by numerous interfaces and structural vacancies (the presence of vacancies is due to a considerable deviation of the chemical composition of the films from stoichiometry; see films Nos 1, 3, 5, 22 and 23 in Table 7). In spite of rather large amounts of oxygen and nitrogen impurities in the films, the character of the ρ-*vs*.-temperature plots for the films Nos 1, 3 and 5 shows that the films remain metal-like systems.[88]

Films based on ZrB_2 have been less studied compared to those based on TiB_2 and HfB_2; therefore, additional studies on their physicomechanical properties are needed.

By and large, the measured strength and fracture toughness of sintered microstructured samples of titanium dibor-

Table 7. Selected physicomechanical properties of nano- and microdisperse Ti, Zr and Hf diborides and composites based on them.

No.	Composition	Grain size /nm	H_V /GPa	E /GPa	ρ /μΩ cm	Ref.
Titanium diboride films						
1	$Ti(B_{0.73}N_{0.2}O_{0.05}C_{0.02})_{1.56}$	4–8	~49	460 ± 50	155	88
2		4–8	42 [a]	475 [a]	–	89
3	$Ti(B_{0.69}N_{0.24}O_{0.04}C_{0.03})_{1.64}$	3.6 ± 1.8	~37	430 ± 50	160	88
4	$Ti(B_{0.56}N_{0.29}O_{0.05}C_{0.1})_{1.32}$	2.3 ± 1.1	~49	–	–	86
5	$Ti(B_{0.34}N_{0.49}O_{0.12}C_{0.05})_{1.49}$	2.9 ± 1.1	~49	480 ± 100	255	88
6		2.9 ± 1.1	27.5 [a]	320 [a]	–	89
7	75 TiB_2 + 25 B_4C (see [b])	2.9 ± 0.3	~56	–	–	85
8	50 TiB_2 + 50 B_4C (see [b])	see [c]	~64	–	–	85
9	25 TiB_2 + 75 B_4C (see [b])	2.9 ± 0.3	~66	–	–	85
10	$TiB_{2.4}$	~20	60–70	–	–	65, 72
11		~20	48.5 [a]	600 [a]	–	65, 72
12	33 TiB_2 + 66 TiN (see [b])	2–4	24–34 [a]	220–380 [a]	–	90
13	5 TiB_2 + 95 W_2B_5 (see [b])	~4	34.6 [a]	323 [a]	–	91
14	TiN/BN/TiB_2 (see [d])	~10	~48	–	–	81
15	TiB_2	2–7	48.6 [a]	562 [a]		77
Sintered titanium diboride samples						
16	TiB_2 + 2.5 Ti	8×10^3	26.8 ± 1.6	–	–	60
17	TiB_2	$(1.6–4.9) \times 10^3$	23–24.5	468–520	8.5–12.2	56, 92
18	TiB_2 + ~10 TiB	3×10^3	18.3	428	13.8	58
19	36 TiB_2 + 64 TiN	$(0.2–0.3) \times 10^3$	24.6–26.2	432–440	13–14	92
20	50 TiB_2 + 50 TiN	$(0.25) \times 10^3$	25.6 ± 0.4	450 ± 10	13	92
Zirconium diboride films						
21	$ZrB_{2.5–2.9}$	–	~23	–	–	93, 94
22	$ZrB_{1.84–2.0}$	–	–	–	95–200	78
23	ZrB_2	36 (see [e])	–	–	20	79
24	ZrB_2	–	~22.5 [a]	~290 [a]	–	95
25	ZrB_2/AlN (see [d])	4–18	18–23 [a]	260–300 [a]	–	95
Sintered zirconium diboride samples						
26	70 ZrB_2 + 15 SiC + 15 B_4C (see [f])	$(3–10) \times 10^3$	20.2 ± 0.9	522 ± 18	–	96
27	4 ZrB_2 + 33 SiC + 33 B_4C (see [f])	$(1–10) \times 10^3$	28.9 ± 1.6	538 ± 36	–	96
Hafnium diboride films						
28	HfB_2	12	40 [a]	430 [a]	–	69
29		see [c]	~20 [a]	~330 [a]	–	69
30	HfB_2 – HfN – BN	–	~16 [a]	~200 [a]	–	69
31	HfB_2/Hf(B,N) (see [f])	2/10	~33 [a]	~300 [a]	–	69
32	$HfB_{1.8–2.4}$	10–20	26–44 [a]	254–584 [a]	–	71
		see [c]	12.6 ± 2.6 [a]	177 ± 26 [a]	–	71
33	Hf(B,N)	–	9.3–9.4 [a]	157–176 [a]	–	71
Sintered hafnium diboride samples						
34	HfB_2 + 30 SiC (see [f])	~2×10^3	26 ± 1	512 ± 4	–	97
35	HfB_2 + 20 SiC (see [f])	~2×10^3	20.2 ± 1	–	–	98
36	HfB_2 + 15 $MoSi_2$ (see [f])	~1.5×10^3	20.6 ± 0.4	530 ± 5	–	99

[a] Nanoindentation data. [b] Target composition (mass %). [c] Amorphous structure. [d] Multilayer films. [e] Single-crystal thickness. [f] Composition of the samples (vol.%).

ide and TiB_2 + TiN and TiB_2 + TiC composites[92, 101] are no higher than 400–500 MPa and 5–6 MPa $m^{1/2}$, respectively. Textured, hot-pressed microstructured samples of composition ZrB_2 + 20 vol.% SiC are characterized by higher σ_b values up to 720–790 MPa (loading along c axis).[62, 102] High-temperature strength studies showed that the advantages of textured samples are retained up to 1650 °C.[102] In a wide temperature range up to 2300 °C, the temperature dependences of σ_b measured for ZrB_2 and many other refractory compounds[17] are nonmonotonic and the samples show no indications of plasticity.[103] An electron microscopy study of the fracture surfaces of the samples tested at different temperatures showed that raising the temperature causes the character of fracture to change from transcrystalline to intercrystalline or mixed (samples comprised of smaller grains exhibit some plasticity).[102]

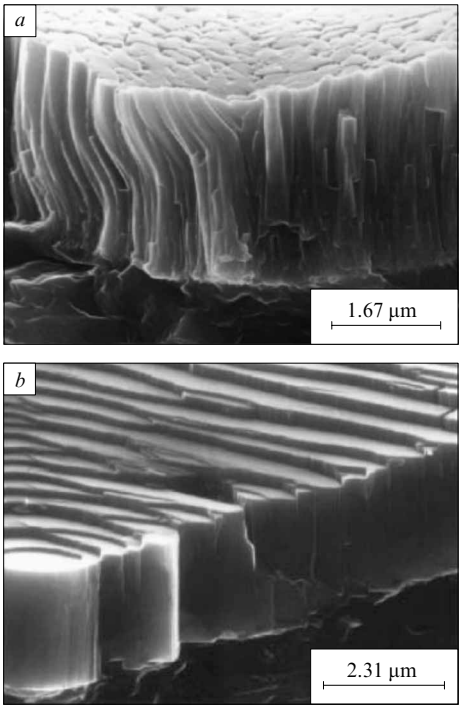


Figure 12. Fractogram and indentation imprint surface in TiN (*a*) and TiB_2 (*b*) films near the indenter puncture.[100, 107]
Residual plastic deformation of a number of TiN nanocolumns (*a*) and the formation of steps for the TiB_2 film (*b*).

Manifestation of superplasticity in pseudobinary coarse-grained eutectic composites TiB_2-TiC and ZrB_2-ZrN under high-temperature creep (at 2200 – 2300 °C) and in the measurements of microhardness in the HfB_2-HfN system were established more than four decades ago (see a review of superplasticity studies of refractory compounds in the handbook [17]); however, these studies did not go to any further. To date, indications of plasticity and superplasticity are known for a limited number of nanostructured refractory compounds (*e.g.*, in the microhardness measurements of nanocolumnar TiN films and in the *in situ* electron microscopy observations of bending of SiC nanowires).[100, 104 – 106] Experiments on detection of plasticity and superplasticity in nanostructured diborides are still a matter of the future. In this connection, high-resolution SEM may appear to be useful because the method enables monitoring of subtle details of deformation and fracture, as illustrated in Fig. 12.

III.3. The heating, irradiation, deformation and corrosion behaviour of diboride nanostructures

Since nanostructures have numerous interfaces (and, correspondingly, an excess free energy), attention is being increasingly focused on the stability studies of these systems.[3, 4, 67, 108] Presently, research into the stability of titanium, zirconium and hafnium diborides is in the early stage, the stability of nitride films being studied in more detail.[65, 109 – 111] The plots of hardness *vs.* annealing temperature (see Fig. 13) show that superstoichiometric $TiB_{2.4}$ films are much more stable that TiN films and retain high hardness up to 30-min annealing at 800 °C.[83] Ti(B,N) and $TiB_2 + TiN$ films were also reported to be stable in this

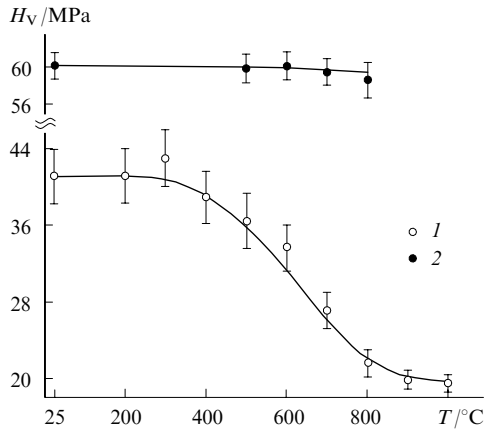


Figure 13. Vickers hardness of TiN (*1*) and $TiB_{2.4}$ (*2*) films plotted *vs.* annealing temperature.[83]

temperature range;[65, 83, 86, 87] however, diboride films are less stable than multicomponent nitride systems (*e.g.*, TiAlSiCN) whose thermal stability region spans to about 1300 °C.[111]

The interest in the microcomposites based on ZrB_2 and HfB_2 is, in particular, due to the search for high-temperature oxidation-resistant materials for nose caps and leading edges of space crafts.[12, 52] Broad-scale research on the oxidation and strength degradation of these systems containing various additives, such as SiC, $MoSi_2$, $TaSi_2$, WSi_2, *etc.* is in progress. At high temperatures (see, *e.g.*, Refs 63 and 112 – 117); however, the role of the microstructural size effects (say nothing of nanostructural ones) is still almost ignored.

A review of studies on the size effects manifesting themselves in the interaction of nanomaterials with the environment is available,[118] but information concerning nanostructured refractory compounds in general and, in particular, titanium, zirconium and hafnium diborides is scarce. An *ab initio* density functional theory study [119] of the interaction of titanium diboride in the form of nanocrystals and different surfaces [(0001) and $(01\bar{1}0)$ planes] with hydrogen, oxygen and water molecules predicted that TiB_2 is expected to be stable in these corrosion media. Electrochemical properties of amorphous nanocrystalline TiB_2 films in 3% NaCl solution simulating the influence of sea water were investigated.[120, 121] The samples studied were shown to have a great advantage over coarse-grained samples; also, a pitting corrosion was revealed.

Interest in research on the influence of irradiation on the properties of boride compounds is first of all due to the use of borides as neutron-absorbing materials in nuclear power engineering. A study [122] of structural changes in $Ti_{1-x}B_x$ films ($0.5 \leqslant x \leqslant 0.8$) irradiated by fast and thermal neutrons (maximum fluence to 7.7×10^{24} and 10^{23} neutron m^{-2}, respectively; the maximum dose was equal to ~ 0.5 displacement per atom) showed that irradiation activates manifestation of the $\langle 0001 \rangle$ texture and revealed the appearance of reflections attributable to orthorhombic phases (TiB or Ti_3B_4) in addition to conventional diffraction reflections from TiB_2. When carrying out neutron irradiation experiments with boron and boron compounds, one should take into account not only conventional deformation effects, but also damage due to the appearance of

lithium and helium as a result of transmutation. An estimation[122] showed that at a thermal neutron fluence of 10^{25} neutron m^{-2}, nearly 19% of ^{10}B atoms will be transmuted in the (n, α) reaction and thus the stoichiometric TiB_2 will transform to $TiB_{1.6}$ and may assist formation of TiB or Ti_3B_4 phases. Also, the concentration of helium generated from the (n, α) reaction was estimated to be nearly 19 at.%, which causes an increase in the lattice constants and development of internal stress.

Experiments with irradiation of TiB_2 (films and hot-pressed samples) and HfB_2 (sintered samples) with different ions at irradiation devices made it possible to reveal specific features of deuterium desorption from various media and to revise the laws of swelling and hardening in the irradiated samples.[123, 124] Taking into account the results of studies on the influence of irradiation on the properties of nanostructured monolayer and multilayer nitride films,[125, 126] one can expect that nanosized diboride samples will also be characterized by low swelling and radiation hardening owing to accelerated removal of radiation-induced defects along numerous interfaces.

The behaviour of titanium diboride under shock compression and high-energy ball milling was studied.[127, 128] On the one hand, no phase transformations at pressures up to 120 GPa was observed.[127] On the other hand, a SEM and HR TEM study of the structural evolution of TiB_2 under high external stresses revealed the presence of lamellar nanotwins and dislocations that can be treated as evidence of plastic deformation in microcrystals.[128]

IV. Conclusion

Information on nanostructured titanium, zirconium and hafnium diborides presented in this review is of different type and quality and mainly concerns the development of methods for synthesis of nanopowders and films. Data on consolidation of powders and on the role of the size effects in these processes are still scarce and empirical. Since nanomaterials based on transition-metal borides have a potentially wide field of application, the highest-performance methods for the synthesis of boride nanopowders should be optimized and the possibility of consolidation of these materials with retention of nanostructure should be considered in detail.

Seemingly, prospects for basic research are also great. For comparison, mention may be made that, theoretically, studies on magnesium diboride nanotubes and diamond films are more advanced and fruitful; they led to establishment of correlations between the stability of physical properties and the size effects (see, *e.g.*, Refs 129 and 130). Investigations of the low-temperature electronic heat capacity and paramagnetic susceptibility of nanoscale diborides could contribute largely to understanding a possible evolution of the electronic energy spectrum; these parameters can be used to refine the density of states at the Fermi level in these systems. The need for other physicochemical studies was emphasized above.

Undoubtedly, extension of research on nanostructured Group IV transition-metal diborides will not only provide useful information that is necessary for deeper insight into the nature of nanostructures, but also be basic to significant extension of applied R&D in various areas of technology.

The author of this review is grateful to V V Klyucharev and S V Klyucharev for help in preparing the manuscript for publication. The review has been written with the financial support from the Presidium of the Russian Academy of Sciences (Basic Research Programme No. 1), the Materials Science Division of the Russian Academy of Sciences (Programme No. 8) and the Russian Foundation for Basic Research (Project No.13-03-01014).

References

1. *Sol. St. Sci., Special Issue* **14** (11–12) 1559 (2012)
2. S Carenco, D Portehault, C Boissiere, N Mezailles, C Sanchez *Chem. Rev.* **113** 7981 (2013)
3. R A Andrievski *Russ. Chem. Rev.* **83** 465 (2014)
4. R A Andrievski *Osnovy Nanostrukturnogo Materialovedeniya. Vozmozhnosti i Problemy* (Fundamentals of Nanostructural Sciences of Material. Resources and Problems) (Moscow: Binom. Laboratoriya Znanii, 2012)
5. R A Andrievski *Russ. Chem. Rev.* **78** 821 (2009)
6. R A Andrievski *Russ. Chem. Rev.* **81** 549 (2012)
7. Yu B Kuz'ma, N F Chaban *Dvoinye i Troinye Sistemy, Soderzhashchie Bor. Spravochnik* (Binary and Ternary Systems Containing Boron. Handbook) (Moscow: Metallurgiya, 1990)
8. T I Serebryakova, V A Neronov, P D Peshev *Vysokotemperaturnye Boridy* (High-Temperature Borides) (Chelyabinsk: Metallurgiya, 1991)
9. G Cacciamani, P Riani, F Valenza *Calphad* **35** 601 (2011)
10. H M Chen, F Zheng, H S Liu, L B Liu, Z P Jin *J. Alloys Compd.* **468** 209 (2009)
11. J Hu, X Dong, S Tosto *J. Am. Ceram. Soc.* **95** 2089 (2012)
12. W G Fahrenholtz, G E Hilman, I G Talmy, J A Zaykoski *J. Am. Ceram. Soc.* **90** 1347 (2007)
13. L Sun, Y Gao, B Xiao, Y Li, G Wang *J. Alloys Compd.* **579** 457 (2013)
14. R A Andrievski Ya S Umanskii *Fazy Vnedreniya* (Interstitial Alloys) (Moscow: Nauka, 1977)
15. B Basu, K Balani *Advanced in Structural Ceramics* (Hoboken, NJ: Wiley, 2011)
16. R G Munro *J. Res. Natl. Inst. Stand. Technol.* **105** 709 (2000)
17. R A Andrievski, I I Spivak *Prochnost' Tugoplavkikh Soedinenii i Materialov na ikh Osnove. Spravochnik* (Strength of Refractory Compounds and Materials Based on Them) (Chelyabinsk: Metallurgiya, 1989)
18. A L Ivanovskii, N I Medvedeva, G P Shveikin, Yu E Medvedeva, A E Nikiforov *Metallofiz. Noveishie Tekhnol.* **20** 41 (1998) [a]
19. A L Ivanovskii, N I Medvedeva *Russ. J. Inorg. Chem.* **45** 1355 (2000) [*Zh. Neorg. Khim.* **45** 1355 (2000)]
20. A L Ivanovskii *Prog. Mater. Sci.* **57** 184 (2012)
21. R A Andrievski *Russ. Chem. Rev.* **74** 1061 (2005)
22. R A Andrievski, in *Materials Handbook* (Ed. Y Gogotsi) (Boca Raton, FL: CRC Press, 2006) p. 405
23. A K Khanra, L C Pathak, M M Godkhindi *Adv. Appl. Ceram.* **106** 155 (2007)
24. J W Kim, J-H Shim, J-P Ahn, Y W Cho, J-H Kim, K H Oh *Mater. Lett.* **62** 2461 (2008)
25. E Bilgi, H Erdem Camurlu, B Akgün, Y Topkaya, N Sevinç *Mater. Res. Bull.* **43** 873 (2008)
26. K Nishiyama, T Nakamura, S Utsumi, H Sakai, M Abe *J. Phys. Conf. Ser.* **176** 012043 (2009)
27. H E Camurlu, F Maglia *J. Eur. Ceram. Soc.* **29** 1501 (2009)
28. A L Chamberlain, W G Fahrenholtz, G E Hilmas *J. Eur. Ceram. Soc.* **29** 3401 (2009)
29. F Huang, Z Fu, A Yan, T Jia, W Wang, H Wang, Y Wang, J Zhang, Q Zhang *Mater. Sci. Forum* **620–622** 525 (2009)
30. S Ran, O V Biest, J Vieugels *J. Am. Ceram. Soc.* **93** 1586 (2010)

31. W Ye, P A Peña Martin, N Kumar, S R Daly, A A Rockett, J R Abelson, G S Girolami, J W Lyding *ACS Nano* **4** 6818 (2010)
32. D Portehault, S Devi, P Beaunier, C Gervais, C Giordano, C Sanchez, M Antonietti *Angew. Chem., Int. Ed.* **50** 3262 (2011)
33. M Ramachandran, R G Reddy *J. Manuf. Sci. Prod.* **11** 15 (2011)
34. Y Cheng, T Watanabe *J. Chem. Eng. Jpn.* **44** 583 (2011)
35. Patent RF 2465096 (2012)
36. M A Aviles, J M Cordoba, M J Sayagues, F J Gotor *Ceram. Int.* **37** 1895 (2011)
37. W-M Guo, Z-G Yang, G-J Zhang *Mater. Lett.* **93** 52 (2012)
38. H Wang, S-H Lee, H-D Kim *J. Am. Ceram. Soc.* **95** 1493 (2012)
39. V Zamora, A L Ortiz, F Guiberteau, M Nygren *J. Eur. Ceram. Soc.* **32** 271 (2012)
40. S Guo, D H Ping, Y Kagawa *Ceram. Int.* **38** 5195 (2012)
41. L S Volkova, Yu M Shul'ga, S P Shilkin *Russ. J. Gen. Chem.* **82** 819 (2012) [*Zh. Obshch. Khim.* **82** 709 (2012)]
42. L S Volkova, S E Kravchenko, I I Korobov, A M Kolesnikova, N N Dremova, A G Burlakova, G V Kalinnikov, S P Shilkin *Inorg. Mater.* **49** 1086 (2013) [*Neorg. Mater.* **49** 1173 (2013)]
43. L S Volkova, A G Burlakova, S E Kravchenko, S P Shilkin *Inorg. Mater.* **49** 1187 (2013) [*Neorg. Mater.* **49** 1285 (2013)]
44. S-H Lee, J-Y Yun, H C Oh, J-H Kim, H D Kim *J. Ceram. Soc. Jpn.* **121** 480 (2013)
45. W-W Wu, G-J Zhang, Y Sakka *J. Asian Ceram. Soc.* **1** 304 (2013)
46. F Li, Z Kang, X Huang, G-J Zhang *Chem. Eng. J.* **234** 184 (2013)
47. V V Ivanov, I A Blokhina, S D Kirik *Russ. J. Appl. Chem.* **86** 1650 (2013) [*Zh. Prikl. Khim.* **86** 1698 (2013)]
48. B Nasiri-Tabrizi, T Adhami, R Ebrahimi-Kahrizsangi *Ceram. Int.* **40** 7345 (2014)
49. S Klébert, A M Keszler, I Sajó, E Drotár, I Bertóti, E Bódis, P Fazekas, Z Károly, J Szépvölgyi *Ceram. Int.* **40** 3925 (2014)
50. L S Walker, E L Corral *J. Am. Ceram. Soc.* **97** 399 (2014)
51. S Venugopal, A Paul, B Vaidhyanathan, J G P Binner, A Heaton, P M Brown *J. Eur. Ceram. Soc.* **34** 1471 (2014)
52. J K Sonber, A K Suri *Adv. Appl. Ceram.* **110** 321 (2011)
53. T Tayeh, J Douin, S Jouannigot, M Zakhour, M Nakhl, J-F Silvain, J-L Bobet *Mater. Sci. Eng, A* **591** 1 (2014)
54. R A Andrievskii *Powder Metall. Met. Ceram.* **50** (1 – 2) 2 (2011) [*Poroshk. Metallurg.* (1 – 2) 5 (2011)
55. G J K Harrington, G E Hilmas, W G Fahrenholtz *J. Am. Ceram. Soc.* **96** 3622 (2013)
56. D Demirskyi, J Cheng, D Agrawal, A Ragulya *Scr. Mater.* **69** 610 (2013)
57. V Zamora, A L Ortiz, F Guiberteau, M Nygren *J. Eur. Ceram. Soc.* **32** 2529 (2012)
58. A Mukhopadhyay, T Venkateswaran, B Basu *Scr. Mater.* **69** 159 (2013)
59. L Wang, J Zhang, W Jiang *Int. J. Ref. Met. Hard. Mater.* **39** 103 (2013)
60. Z-H Zhang, X-B Shen, F C Wang, S-K Lee, Q-B Fan, M-S Cao *Scr. Mater.* **66** 167 (2012)
61. C Tallon, D Chavara, A Gillen, D Riley, L Edwards, S Morrica, G V Franks *J. Am. Ceram. Soc.* **96** 2374 (2013)
62. H-T Liu, G-J Zhang *J. Ceram. Soc. Jpn.* **121** 327 (2013)
63. W-W Wu, Y Sakka, T S Suzuki *Int. J. Appl. Ceram. Technol.* **11** 218 (2014)
64. R A Andrievskiy *Russ. Chem. Rev.* **66** 53 (1997)
65. P H Mayrhofer, C Mitterer, L Hultman, H Clemens *Prog. Mater. Sci.* **51** 1032 (2006)
66. R A Andrievskii, G V Kalinnikov *Russ. Chem. Bull., Int. Ed.* **60** 1025 (2011) [*Izv. Akad. Nauk, Ser. Khim.* 1001 (2011)]
67. *Nanostructured Coatings* (Eds A Cavaleiro, J T M de Hosson) (New York: Springer, 2006)
68. Y Yang, S Jayaraman, D Y Kim, G S Girolami, J R Abelson *J. Cryst. Growth* **294** 389 (2006)
69. S Jayaraman, J E Gerbi, Y Yang, D Y Kim, A Chatterjee, P Bellon, G S Girolami, J P Chevalier, J R Abelson *Surf. Coat. Technol.* **200** 6629 (2006)
70. S Babar, N Kumar, P Zhang, J R Abelson, A C Dunbar, S R Daly, G S Girolami *Chem. Mater.* **25** 662 (2013)
71. A A Goncharov, S N Dub, A V Agulov *Phys. Met. Metallogr.* **114** 95 (2013) [*Fiz. Met. Metalloved.* **114** 105 (2013)]
72. A A Goncharov *Phys. Metal Metallogr.* **111** 314 (2011) [*Fiz. Met. Metalloved* **111** 325 (2011)]
73. N Kalfagiannis, G Volonakis, L Tsetseris, S Logothetidis *J. Phys. D* **44** 385402 (2011)
74. C M T Sanchez, B Rebollo Plata, M E H Mala da Costa, F L Freire Jr *Surf. Coat. Technol.* **205** 3698 (2011)
75. F Bulbul, I Efeoglu *Surf. Rev. Lett.* **19** 125045 (2012)
76. M Xia, H Ding, G Zhou, Y Zhang, G Zhuang *Adv. Mater. Res.* **647** 697 (2013)
77. F Lofaj, T Moskalewicz, G Cempura, M Mikula, J Dusza, A Czyrska-Filemonowicz *J. Eur. Ceram. Soc.* **33** 2347 (2013)
78. L Tengdelius, M Samuelsson, J Jensen, J Lu, L Hultman, U Forsberg, E Janzen, H Högberg *Thin Solid Films* **550** 285 (2014)
79. S Bera, Y Sumiyoshi, Y Yamada-Takamura *J. Appl. Phys.* **106** 063531 (2009)
80. A Fleurence, Y Yamada-Takamura *Phys. Status Solidi, C* **8** 779 (2011)
81. P Karvankova, M G J Veprek-Heijman, D Azinovic, S Veprek *Surf. Coat. Technol.* **200** 2978 (2006)
82. P H Mayrhofer, C Mitterer, J G Wen, J E Greene, J Petrov *Appl. Phys. Lett.* **86** 131909 (2005)
83. P H Mayrhofer, C Mitterer, H Clemens *Adv. Eng. Mater.* **7** 1071 (2005)
84. R A Andrievski, G V Kalinnikov *Glass Phys. Chem.* **33** 344 (2007) [*Fiz. Khim. Stekla* **33** 483 (2007)]
85. G V Kalinnikov, R A Andrievski, V N Kopylov, D Louzguine *Phys. Solid State* **50** 374 (2008) [*Fiz. Tv. Tela* **50** 359 (2008)]
86. R A Andrievski, G V Kalinnikov, A E Oblezov, D V Shtanski *Dokl. Phys.* **47** 353 (2002) [*Dokl. Akad. Nauk* **384** 36 (2002]
87. R A Andrievski, G V Kalinnikov, in *Nanostructured Thin Films and Nanodispesion Strengthened Coatings* (Eds A A Voevodin, D V Shtansky, E A Levashov, J J Moore) (Dordrecht: Kluwer Academic, 2004) p. 175
88. R A Andrievskii, G V Kalinnikov, N P Kobelev, Y M Soyfer, D V Shtanskii *Phys. Solid State* **39** 1661 (1997) [*Fiz. Tv. Tela* **39** 1859 (1997)]
89. R A Andrievskii, G V Kalinnikov, N Hellgren, P Sandstrom, D V Shtanskii *Phys. Solid State* **42** 1671 (2000) [*Fiz. Tv. Tela* **42** 1624 (2000)]
90. D V Shtansky, F V Kiryukhantsev-Korneev, A N Sheveiko, I A Bashkova, O V Maloshkin, E A Levashov, N B Dyakonova, I V Lyasotskiy *Phys. Solid State* **47** 252 (2005) [*Fizika Tv. Tela* **47** 242 (2005)]
91. O V Sobol *Phys. Solid State* **49** 1161 (2007) [*Fiz. Tv. Tela* **49** 1104 (2007)]
92. D Demirskyi, D Agrawal, A Ragulya *Ceram. Int.* **40**. 1303 (2014)
93. S Mitterer, P Losbichler, W S M Werner, H Störi, J Barounig *Surf. Coat. Technol.* **54/55** 329 (1992)
94. S Mitterer, J Komenda-Stallmaier, P Losbichler, P Schmölz, W S M Werner, H Störi *Vacuum* **46** 1281 (1995)
95. D J Li, M Tan, G Q Liu, H Liu, X Sun *Surf. Coat. Technol.* **205** 3791 (2011)
96. W G Fahrenholtz, E W Neuman, H J Brown-Shaklee, G E Hilmas *J. Am. Ceram. Soc.* **93** 3580 (2010)
97. F Monteverde, C Melandri, S Guicciardi *Mater. Chem. Phys.* **100** 513 (2006)

98. G-J Zhang, W-M Guo, D-W Ni, Y-M Kan, in *The 16th International Sumposium on Boron, Borides and Related Materials (ISSB 2008) Book Series: Journal of Physics Conference Series, Matsue, Japan, 2009* Vol. 176, p. 012041
99. D Scitti, L Silvestroni, A Bellosi *J. Mater. Res.* **21** 1460 (2006)
100. R A Andrievski, A M Glezer *Physics-Uspechi* **52** 315 (2009) [*Usp. Fiz. Nauk* **179** 337 (2009)]
101. D Wang, H Wang, S Sun, X Zhu, G Tu *Thin J. Mater. Sci.* **27** 489 (2013)
102. W-W Wu, Y Sakka, M Estili, T S Suzuki, T Nishimura, G-J Zhang *Sci. Technol. Adv. Mater.* **15** 014202 (2014)
103. E W Neuman, G E Hilmas, W G Fahrenholtz *J. Am. Ceram. Soc.* **96** 47 (2013)
104. R A Andrievski *Bull. Russ. Acad. Sci., Phys.* **73** 1222 (2009) [*Izv. Akad. Nauk, Ser. Fiz.* **73** 1290 (2009)]
105. X D Han, Y F Zhang, K Zheng, X N Zhang, Z Zhang, Y J Hao, X Y Guo, J Yuan, Z L Wang *Nano Lett.* **7** 452 (2007)
106. Y Zhang, X Han, K Zheng, Z Zhang, X Zhang, J Fu, Y Ji, Y Hao, X Guo, Z Wang *Adv. Funct. Mater.* **17** 3435 (2007)
107. R A Andrievski, G V Kalinnikov, J Jaberteau, J Bates *J. Mater. Sci.* **35** 2799 (2000)
108. R A Andrievski *J. Mater. Sci.* **49** 1449 (2014)
109. L Hultman, C Mitterer, in *Nanostructured Coatings* (Eds A Cavaleiro, J T M de Hosson) (New York: Springer, 2006) p. 464
110. J Musil *Surf. Coat. Technol.* **207** 50 (2012)
111. D V Shtansky, K A Kutsov, Ph V Kiryukhantsev-Korneev, A N Sheveyko *Surf. Coat. Technol.* **206** 4840 (2012)
112. D Sciti, M Brach, A Bellosi *Scr. Mater.* **53** 1297 (2005)
113. D-W Ni, G-J Zhang, Y-M Kan, T Sakka *Scr. Mater.* **60** 913 (2009)
114. O N Grigoriev, B A Galanov, V A Lavrenko, A D Panasyuk, S M Ivanov, A V Koroteev, K G Nickel *J. Eur. Ceram. Soc.* **30** 2397 (2010)
115. C Carney, A Paul, S Venugopal, T Parthasarathy, J Binner, A Katz, P Brown *J. Eur. Ceram. Soc.* **34** 1045 (2014)
116. L Silvestroni, G Meriggi, D Sciti *Corrosion Sci.* **83** 281 (2014)
117. L Silvestroni, D Sciti *J. Alloys Compd.* **602** 346 (2014)
118. R A Andrievskii *Prot. Met. Phys. Chem. Surf.* **49** 528 (2013) [*Fizikokhim. Poverkh. Zashch. Mater.* **49** 491 (2013)]
119. G Volonakis, L Tsetserts, S Logothetidis *Mater. Sci. Eng., B* **176** 484 (2011)
120. A S Dranenko, V A Lavrenko, V N Talash *Powder Metall. Metal. Ceram.* **49** (3 – 4) 174 (2010) [*Poroshk. Metallurg.* (3 – 4) 63 (2010)]
121. X Pan, K Shen, J Xu, L Liu *Chin. J. Electr. Dev.* **35** 135 (2012)
122. T Shikama, H Kayano *J. Nuclear Mater.* **179 – 181** 465 (1991)
123. P Cheminant-Coatanlem, L Boulanger, X Deschanels, A Thorel *J. Nucl. Mater.* **256** 180 (1998)
124. T Hino, Y Hashiba, Y Yamauchi, K Nashimura, N Ashikawa, A Sagara, N Noda, A Komori, O Motojima *Fusion Eng. Des.* **85** 655 (2010)
125. R A Andrievski *Nanotechnol. Russ.* **6** 357 (2011) [*Ros. Nanotekhnol.* **6** (5 – 6) 34 (2011)]
126. I Kim, L Jiao, F Khatkhatay, M S Martin, J Lee, L Shao, X Zhang, J G Swadener, Y Q Wang, J Gan, J I Cole, H Wang *J. Nuclear Mater.* **441** 47 (2013)
127. Y Zhang, K Fukuoka, M Kikuchi, M Kodama, K Shibata, T Mashimo *Int. J. Impact Eng.* **32** 643 (2005)
128. F Huang, Z Fu, A Yan, W Wang, H Wang, J Zhang, Q Zhang *Powder Technol.* **197** 83 (2010)
129. P B Sorokin, L A Chernozatonskii, P V Avramov B I Yakobson *J. Phys. Chem. C* **114** 4852 (2010)
130. A G Kvashnin, L A Chernozatonskii, B I Yakobson, P B Sorokin *Nano Lett.* **14** 676 (2014)

[a] — *Met. Phys. Adv. Technol. (Engl. Transl.)*